

Solution NMR Structure of the 48-kDa IIA^{Mannose}-HPr Complex of the *Escherichia coli* Mannose Phosphotransferase System*

Received for publication, February 22, 2005, and in revised form, March 22, 2005
Published, JBC Papers in Press, March 23, 2005, DOI 10.1074/jbc.M501986200

David C. Williams, Jr.‡, Mengli Cai‡, Jeong-Yong Suh‡, Alan Peterkofsky§, and G. Marius Clore‡¶

From the ‡Laboratory of Chemical Physics, NIDDK, and the §Laboratory of Cell Biology, NHLBI, National Institutes of Health, Bethesda, Maryland 20892

The solution structure of the 48-kDa IIA^{Man}-HPr complex of the mannose branch of the *Escherichia coli* phosphotransferase system has been solved by NMR using conjoined rigid body/torsion angle-simulated annealing on the basis of intermolecular nuclear Overhauser enhancement data and residual dipolar couplings. IIA^{Man} is dimeric and has two symmetrically related binding sites per dimer for HPr. A convex surface on HPr, formed primarily by helices 1 and 2, interacts with a deep groove at the interface of the two subunits of IIA^{Man}. The interaction surface on IIA^{Man} is predominantly helical, comprising helix 3 from the subunit that bears the active site His-10 and helices 1, 4, and 5 from the other subunit. The total buried accessible surface area at the protein-protein interface is 1450 Å². The binding sites on the two proteins are complementary in terms of shape and distribution of hydrophobic, hydrophilic, and charged residues. The active site histidines, His-10 of IIA^{Man} and His-15 (italics indicate HPr residues) of HPr, are in close proximity. An associative transition state involving a pentacoordinate phosphoryl group with trigonal bipyramidal geometry bonded to the N-ε2 atom of His-10 and the N-δ1 atom of His-15 can be readily formed with negligible displacement in the backbone coordinates of the residues immediately adjacent to the active site histidines. Comparing the structures of complexes of HPr with three other structurally unrelated phosphotransferase system proteins, enzymes I, IIA^{glucose}, and IIA^{mannitol}, reveals a number of common features that provide a molecular basis for understanding how HPr specifically recognizes a wide range of diverse proteins.

The bacterial phosphoenolpyruvate:sugar phosphotransferase system (PTS)¹ provides a signaling network whereby

free energy generated from phosphoryl transfer between successive members of the pathway is transduced to drive the uptake of carbohydrates across the cytoplasmic membrane (1–4). The initial phosphorylation steps from phosphoenolpyruvate to enzyme I, and subsequently to the histidine phosphocarrier protein, HPr, are common to all branches of the pathway. The subsequent phosphorylation steps involve sugar-specific enzymes II, which fall into four major families (glucose, mannitol, mannose, and lactose/chitobiose), that bear no sequence and, in the majority of cases, no structural similarity to one another (2–4). The functional organization, however, of the enzymes II is similar; there are two cytoplasmic domains, IIA and IIB, and a transmembrane sugar permease domain, IIC (and in some instances, IID as well), which may or may not be covalently linked to one another. The protein-protein complexes within the PTS are generally weak and have proved refractory to crystallization. These complexes, in which proteins are able to recognize multiple and structurally diverse partners using similar interaction surfaces, provide a paradigm for understanding the structural basis of protein-protein interactions. In a series of papers, we have reported the solution structures of the enzyme I (N-terminal domain)-HPr complex (5), the two soluble complexes of the glucose branch of the PTS (IIA^{Glc}-HPr (6) and IIA^{Glc}-IIB^{Glc} (7)), and the IIA^{Mtl}-HPr complex of the mannitol branch (8). In the present work, we extended these studies to the solution structure determination of the 48-kDa dimeric IIA^{Man}-HPr complex from the mannose branch of the PTS.

The mannose transporter (II^{Man}) is composed of four domains expressed as two proteins, the soluble IIAB^{Man} component that associates with the integral membrane IICD^{Man} permease (9, 10). The A and B domains of IIAB^{Man} are linked by a 20-residue flexible linker and contain the first (His-10) and second (His-175) phosphorylation sites, respectively, of the II^{Man} complex (11–13). IIA^{Man} accepts a phosphoryl group from HPr and donates it to IIB^{Man}. IIB^{Man} mediates contacts with the transmembrane IICD^{Man} permease and phosphorylates the incoming mannose at the O-6' position. The IIA^{Man} domain is responsible for dimer formation of IIAB^{Man}, and its crystal structure has been solved at 1.7-Å resolution (14). Although the structure of the *Escherichia coli* IIB^{Man} domain has not been solved to date, crystal structures of the homologous IIB^{levulose} (15) and IIB^{sorbitose} (16) domains have been determined. The availability of high resolution crystal structures for both *E. coli* IIA^{Man} (14) and HPr (17) permitted us to solve the solution NMR structure of the IIA^{Man}-HPr complex using conjoined rigid body/torsion angle-simulated annealing on the basis of

* This work was supported in part by the AIDS Targeted Anti-viral Program of the Office of the Director of the National Institutes of Health (to G. M. C.). The costs of publication of this article were defrayed in part by the payment of page charges. This article must therefore be hereby marked "advertisement" in accordance with 18 U.S.C. Section 1734 solely to indicate this fact.

The atomic coordinates and the experimental NMR restraints (code 1VRC) have been deposited in the Protein Data Bank, Research Collaboratory for Structural Bioinformatics, Rutgers University, New Brunswick, NJ (<http://www.rcsb.org/>).

¶ To whom correspondence should be addressed: Laboratory of Chemical Physics, Bldg. 5, Rm. B1-301, NIDDK, NIH, Bethesda, MD 20892-0520. Tel.: 301-496-0782; Fax: 301-496-0825; E-mail: mariusc@intra.niddk.nih.gov.

¹ The abbreviations used are: PTS, phosphotransferase system; RDC, residual dipolar coupling; SVD, singular value decomposition; NOE, nuclear Overhauser effect; HPr, histidine-containing phosphocarrier protein; TROSY, transverse relaxation optimized spectroscopy; EIN, N-terminal domain of enzyme I; r.m.s., root mean square; IIA^{Man}, A

domain of the II^{Man} transporter; IIB^{Man}, B domain of the II^{Man} transporter; IICD^{Man}, integral membrane component of the II^{Man} transporter; IIA^{Glc}, A domain of the glucose transporter; IIA^{Mtl}, A domain of the mannitol transporter.

residual dipolar couplings (RDCs) and intermolecular nuclear Overhauser enhancements (NOEs) (18, 19).

EXPERIMENTAL PROCEDURES

Cloning, Expression, and Purification of IIA^{Man}—*E. coli* chromosomal DNA was used as the template to amplify, by PCR, the region corresponding to the A domain (IIA^{Man}) of the soluble IIA^{BMan} component of the mannose transporter (11). The forward PCR primer 5'-AAGGAGGTAGCATATGACCATTGCTA-3', spanning the region from bases 363 to 388 (NCBI accession number J02699), contained an engineered NdeI site (underlined); the reverse primer 5'-TGGTGCTGCG-GCAGCGGATCCTGGCTATTATTTTTCAACCGGTTT-3', spanning the region from bases 813 to 769, contained an engineered BamHI site (underlined) and a tandem pair of in-frame termination codons (italics). This PCR product was designed to express a peptide encoding amino acid residues Thr-1 to Lys-136 preceded by an N-terminal methionine. The NdeI- and BamHI-cut PCR product was purified and cloned into the corresponding sites of the expression vector pRE1. The selected clone was verified by DNA sequencing. The expression vector was shown to express a protein of the expected size. IIA^{Man} was then subcloned into a modified pET32a vector engineered to express wild-type IIA^{Man} (residues 1–136) without a fusion partner or any additional residues. The recombinant plasmid pSP100 for HPr expression (20) was likewise subcloned into a modified pET32a vector engineered to express wild-type protein (residues 1–85) without a fusion partner or any additional residues.

The recombinant IIA^{Man} and HPr plasmids were introduced into *E. coli* BL21(DE3) cells for protein expression and induced at an A_{600 nm} ~1 with 1 mM isopropyl-β-D-thiogalactopyranoside. Cells were grown in either Luria-Bertani medium, for unlabeled proteins, or in minimal medium (with either H₂O or D₂O, depending on the isotope-labeling scheme) supplemented as appropriate with ¹⁵NH₄Cl, [¹³C₆]glucose, [²H₇]glucose, [²H₇, ¹³C₆]glucose, [¹³C₅, 3-²H₁]α-ketoglutarate, and/or [¹³C₄, 3,3-²H₂]α-ketobutyrate, to generate various isotopically labeled samples. The latter three carbon sources were used to generate (Ile/Leu/Val)-methyl-protonated (but otherwise fully deuterated) ¹³C-labeled protein (21). Two samples of each protein were produced: ¹⁵N/¹³C and ¹⁵N/¹³C/²H/(Ile/Leu/Val)-methyl-protonated IIA^{Man}, and ¹⁵N/¹³C, and ²H/¹⁵N HPr.

Purification of IIA^{Man}—After induction, cells were pelleted, resuspended in 100 ml (per 1 liter of culture) of 20 mM sodium phosphate buffer, pH 7.0, 50 mM NaCl, and 1 mM EDTA, and lysed by three passages through a microfluidizer. The supernatant solution was loaded onto a DEAE-Sepharose anion exchange column in 20 mM sodium phosphate, pH 7.0, and 50 mM NaCl and eluted with a 50-mM to 0.7-M NaCl gradient. The pooled peak containing IIA^{Man} was concentrated and passed through a Superdex-75 gel filtration column equilibrated with 20 mM sodium phosphate, pH 7.0, and 200 mM NaCl. The pooled fractions containing IIA^{Man} were then diluted 1:3 with 20 mM sodium phosphate buffer, pH 7.0, loaded onto a Mono Q anion exchange column, and eluted with a 0–1 M NaCl gradient. Finally, the buffer was exchanged into NMR buffer containing 40 mM sodium phosphate, pH 6.5.

Purification of HPr—Harvested cells were resuspended into 30 ml (per 1 liter of culture) of 6 M guanidinium chloride, 20 mM Tris, pH 8.0, and lysed by sonication. The pellet was spun out and the supernatant solution dialyzed against 20 mM Tris, pH 8.0, and 150 mM NaCl. The pelleted precipitate was then discarded and the supernatant solution subjected to 20% ammonium sulfate precipitation. The resulting supernatant solution was subjected to 80% ammonium sulfate precipitation. The pellet was dissolved in 8 ml of 20 mM Tris, pH 7.5, 200 mM NaCl, and 2 mM EDTA and fractionated on a Superdex-75 gel filtration column in the same buffer. The fractions containing HPr were pooled and exchanged into the NMR buffer (40 mM sodium phosphate, pH 6.5).

NMR Spectroscopy—All complexes (in 40 mM sodium phosphate buffer, pH 6.5, and either 90% H₂O/10% D₂O or 100% D₂O) for NMR were prepared using 1:3 molar ratios in binding sites (0.4–0.5 mM to 1.2–1.5 mM) with the unlabeled protein in excess. Almost all experiments carried out on complexes with isotopically labeled IIA^{Man} or HPr involved uniformly ¹⁵N/¹³C-labeled protein, with the exception of the measurement of dipolar couplings, which made use of complexes comprising either ²H/¹⁵N/¹³C/(Ile/Leu/Val)-methyl-protonated IIA^{Man} or ²H/¹³C-labeled HPr.

NMR spectra were collected at 35 °C on Bruker DMX500, DMX600, DRX600, DMX750, and DRX800 spectrometers equipped with either x,y,z-shielded gradient triple resonance probes or z-shielded gradient triple resonance cryoprobes. Spectra were processed with the NMRPipe

package (22) and analyzed using the programs PIPP/CAPP/STAPP (23).

Sequential and side-chain assignment of free IIA^{Man} was performed using three-dimensional triple resonance through-bond scalar correlation experiments (three-dimensional HNCACB, CBCA(CO)NH, HB-HA(CBCACO)NH, C(CCO)NH, H(CCO)NH, and HNCO) in conjunction with three-dimensional ¹⁵N-, ¹³C-, ¹³C/¹³C-, and ¹⁵N/¹⁵N-separated NOE experiments (24–26). Assignments of free HPr, derived from three-dimensional double and triple resonance experiments, were taken from our work published previously (5, 20) and from Williams and Clore.² Assignments of IIA^{Man} and HPr in the complex were based on the free assignments (minimal chemical shift changes) together with data from three-dimensional HNCO and HNCA triple resonance correlation experiments and three-dimensional ¹³C-, ¹³C/¹³C-, and ¹⁵N-separated NOE experiments. Intermolecular NOEs were recorded on saturated complexes with one partner ¹⁵N/¹³C-labeled and the unlabeled component in 3-fold molar excess of binding sites using three-dimensional ¹³C-separated/¹²C-filtered NOE experiments (26).

Side-chain torsion angle restraints were derived from ³J_{NCγ} and ³J_{CCγ} coupling constants measured using quantitative *J* correlation spectroscopy (27) in conjunction with short mixing time three-dimensional ¹³C-separated NOE spectra (26). The tautomeric states of the active site histidines were confirmed using a long-range heteronuclear single quantum coherence correlation spectrum (28).

Residual Dipolar Couplings—^D_{NH} RDCs were measured by taking the difference in ¹J_{NH} couplings between liquid crystalline (5% polyethylene glycol/hexanol with a surfactant to alcohol ratio of 0.96; (29)) and isotropic (water) media. Small variations in the effective concentration of the liquid crystalline medium between samples were corrected by linear scaling of the measured RDCs based on accurate measurement of the deuterium splitting of the HOD signal. For HPr, a ²H/¹⁵N-labeled sample was employed, and ¹J_{NH} couplings were determined from a two-dimensional TROSY-based (30) heteronuclear single quantum correlation spectrum interleaved to collect the downfield and upfield nitrogen components separately. For IIA^{Man}, a ²H/¹⁵N/¹³C/¹H-methyl-labeled sample was used, and ¹J_{NH} couplings were measured using a three-dimensional HNCO-TROSY-based experiment (31). Further details are discussed in the "Results."

Structure Calculations—NOE-derived interproton distance restraints were classified into loose approximate distance ranges of 1.8–2.7, 1.8–3.5, 1.8–5.0, and 1.8–6.0 Å corresponding to strong, medium, weak, and very weak NOE cross-peak intensities, respectively; an additional 0.5 Å was added to the upper distance bound of distance restraints involving methyl groups (0.5 Å/methyl group). NOEs involving non-stereospecifically assigned methyl, methylene, and aromatic protons were represented by a (Σr⁻⁶)^{-1/6} sum (26). The error range employed for χ₁ torsion angle restraints (represented by square well potentials) was ±20° when a unique rotamer could be identified and ±80° when the torsion angle could be narrowed down to two of the three rotamers.

Structures were calculated using conjoined rigid body/torsion angle-simulated annealing (8, 19) with the program Xplor-NIH (32). The minimized target function comprises the experimental NMR restraints (NOE-derived interproton distances, torsion angles, and residual dipolar couplings), a quartic van der Waals repulsion term for the non-bonded contacts (33), a torsion angle data base potential of mean force (34), and a radius of gyration restraint to ensure optimal packing (35). The latter was applied as two restraints, each comprising one molecule of HPr and both subunits of IIA^{Man}. In addition, non-crystallographic symmetry restraints were applied to ensure that the calculated dimer was fully symmetric.

Best-fitting of the measured RDCs to the crystal structures of free HPr (Protein Data Bank accession code 1POH; 2 Å resolution (17)) and IIA^{Man} (Protein Data Bank accession code 1PDO; 1.7 Å resolution (14)) was carried out by singular value decomposition (SVD) using the program SSIA (36). Structure figures were generated using the programs VMD-XPLOR (37), RIBBONS (38), and GRASP (39). Reweighted atomic probability density maps were calculated as described previously (40).

RESULTS AND DISCUSSION

Binding of HPr to IIA^{Man}—HPr binds to IIA^{Man} with a stoichiometry of two HPr molecules per IIA^{Man} dimer. The interaction is in fast exchange on the chemical shift time scale, and from a maximum chemical shift perturbation of ~600 Hz (for

² D. C. Williams and G. M. Clore, unpublished data.

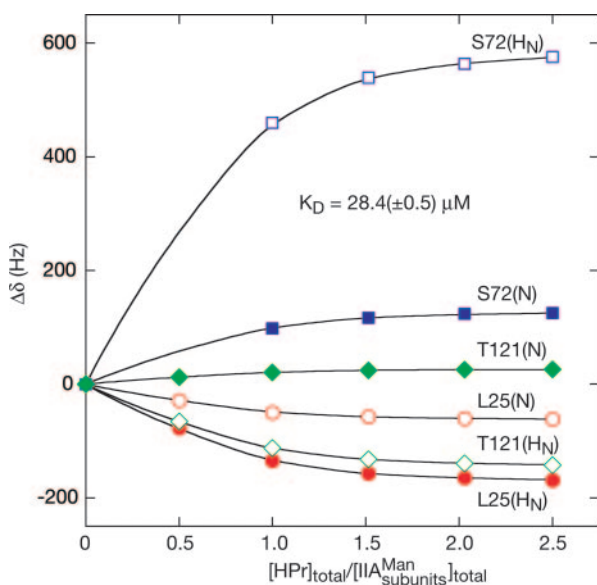


FIG. 1. **Binding of HPr to IIA^{Man}.** Perturbation of backbone ¹⁵N and ¹H_N chemical shifts for three residues (Leu-25, Ser-72, and Thr-121) of IIA^{Man} as a function of added HPr. The continuous curves represent best-fit theoretical curves to all the titration data simultaneously, with an equilibrium dissociation constant of 28.4(± 0.5) μM. The concentration of IIA^{Man} is expressed on a subunit basis (*i.e.* two HPr binding sites per IIA^{Man} dimer).

the backbone amide proton of Ser-72) at a ¹H frequency of 600 MHz, one can deduce that the lifetime of the complex must be less than ~250 μs (*i.e.* << 1/2πΔ_{max}, where Δ_{max} is the maximum observed chemical shift perturbation in Hz). A plot of the chemical shift changes for a number of residues as a function of the molar ratio of HPr to IIA^{Man} subunits is shown in Fig. 1; a simultaneous non-linear least squares fit to all the data yields an equilibrium dissociation constant of 28.4 ± 0.5 μM.

The backbone ¹H_N and ¹⁵N chemical shift perturbations observed upon complex formation are small; only a single residue of IIA^{Man} (Ser-72) exhibits a combined ¹H_N/¹⁵N chemical shift perturbation (Δ_{H/N} = [(Δδ¹H_N)² + (Δδ¹⁵N)²]^{1/2}) in excess of 600 Hz (at a ¹H frequency of 600 MHz); four residues of HPr (Lys-24, Leu-47, Phe-48, Lys-49) exhibit Δ_{H/N} perturbations in the 200–400 Hz range; and three residues of IIA^{Man} (Leu-25, Ala-104, Thr-121) and five residues of HPr (Leu-14, Ala-20, Glu-25, Ala-44, Ser-46) display Δ_{H/N} perturbations in the 100–200 Hz range. These observations, together with the excellent agreement between the measured backbone ¹D_{NH} RDC and those calculated by SVD best-fitting against the crystal structures of free HPr and free IIA^{Man} (see below), indicate that there are no significant perturbations in the backbone coordinates upon complexation within the limits of the NMR method.

Structure Determination—The structure was determined using conjoined rigid body/torsion angle dynamics (8, 19) primarily on the basis of intermolecular NOE data derived from three-dimensional ¹³C-separated/¹²C-filtered NOE experiments and RDCs measured in a liquid crystalline medium of polyethylene glycol/hexanol. These data were supplemented by intramolecular NOE and ³J coupling constant data related to the interfacial side chains. In this approach, the coordinates for the backbone and non-interfacial side chains of the two proteins, taken from the crystal structures of free IIA^{Man} (14) and HPr (17), are treated as rigid bodies that are free to rotate and translate, whereas the interfacial side chains are given full torsional degrees of freedom. The intermolecular NOE-derived interproton distance restraints provide semi-quantitative translational and orientational information, whereas the ¹D_{NH} backbone RDCs (acting in concert, because the backbone con-

formations are fixed) provide highly accurate, quantitative orientational restraints (18, 41). An example of the quality of the intermolecular NOE data is shown in Fig. 2.

In the case of a weak complex with a 1:1 binding stoichiometry, it is a simple matter to obtain samples in which the uniformly, isotopically ¹⁵N- and/or ¹³C-labeled partner is fully bound by ensuring the presence of a suitable excess of the unlabeled partner (5, 6, 8). RDCs for the complex are then measured on the labeled partner, and two samples are employed, with isotope labeling of one partner in one sample and the other partner in the second sample. Under such conditions, the alignment tensors describing the RDCs measured on both samples relate to the same complex and are therefore identical. The situation in the case of the IIA^{Man}-HPr complex, however, is more complicated because IIA^{Man} is a dimer with two equivalent binding sites for HPr. Because the equilibrium dissociation constant for the complex is relatively weak (~28 μM), it is not feasible to obtain a sample in which both HPr and IIA^{Man} are simultaneously fully bound. RDCs recorded on a sample of labeled IIA^{Man} in the presence of excess HPr will exclusively reflect the 1:2 IIA^{Man}(dimer)-HPr complex. However, RDCs recorded on a sample of labeled HPr in the presence of excess IIA^{Man} will arise not from a single species but from a mixture of two species with a stoichiometry of 1:1 and 1:2 IIA^{Man}(dimer) to HPr (*i.e.* one and two HPr binding sites on IIA^{Man} occupied, respectively). The alignment tensors for these two species will necessarily be different and impossible to deconvolute. We therefore recorded RDCs for HPr on a sample comprising labeled HPr in excess over unlabeled IIA^{Man} (with a ratio of 3:1 HPr to IIA^{Man} subunits). Under these conditions, the measured RDCs correspond to a weighted average of the RDCs for two species: free HPr and HPr in the 1:2 IIA^{Man}(dimer)-HPr complex (*i.e.* both HPr sites on IIA^{Man} occupied). The RDCs for the latter can then be readily back-calculated from the experimental data using accurate RDCs measured on free HPr in the same liquid crystalline medium using the relationship,

$$\text{RDC}_{\text{bound},i}^{\text{HPr}} = (\text{RDC}_{\text{obs},i}^{\text{HPr}} - f_{\text{free}}^{\text{HPr}} \text{RDC}_{\text{free},i}^{\text{HPr}}) / (1 - f_{\text{free}}^{\text{HPr}}) \quad (\text{Eq. 1})$$

where $f_{\text{free}}^{\text{HPr}}$ is the fraction of free HPr in the sample, $\text{RDC}_{\text{free},i}^{\text{HPr}}$ are the RDCs measured for free HPr, $\text{RDC}_{\text{obs},i}^{\text{HPr}}$ are the RDCs measured on the sample comprising a 3:1 excess of labeled HPr over IIA^{Man} subunits, and $\text{RDC}_{\text{bound},i}^{\text{HPr}}$ are the back-calculated RDCs for HPr in a pure 1:2 IIA^{Man}(dimer)-HPr complex. (The value of $f_{\text{free}}^{\text{HPr}}$ can be determined accurately from the observed ¹H_N/¹⁵N chemical shift perturbations in the sample because the ¹H_N and ¹⁵N chemical shifts are known in the free and fully bound states.) SVD of the measured backbone ¹D_{NH} RDCs for free HPr against the 2-Å resolution crystal structure of free HPr (17) yields a dipolar coupling *R*-factor, $R_{\text{dip}}^{\text{NH}}$ (42), of 16.7% with a correlation coefficient (r_{corr}) of 0.98 and values of -7.3 Hz and 0.43 for the magnitude of the axial component of the alignment tensor (D_a^{NH}) and rhombicity (η), respectively. The agreement between observed and calculated ¹D_{NH} RDCs for free HPr is well within the range expected for a 2-Å resolution crystal structure (41, 43). The same procedure using the ¹D_{NH} RDCs measured on the sample comprising labeled HPr in 3-fold excess over IIA^{Man} subunits yields $R_{\text{dip}}^{\text{NH}} = 15.4\%$ with $r_{\text{corr}} = 0.97$, $D_a^{\text{NH}} = 5.8$ Hz and $\eta = 0.54$. Using Equation 1, the back-calculated RDCs for HPr in a pure IIA^{Man}(dimer)-HPr 1:2 complex results in $R_{\text{dip}}^{\text{NH}} = 17.6\%$, with $r_{\text{corr}} = 0.97$, $D_a^{\text{NH}} = -28.2$ Hz, and $\eta = 0.031$. Thus, the back-calculated alignment tensor for HPr in the pure IIA^{Man}(dimer)-HPr 1:2 complex is essentially axially symmetric, whereas that for free HPr is rhombic. The back-calculated values of D_a^{NH} and η are in excellent agreement with the values of -28.2 Hz and 0.12, for D_a^{NH} and η , respectively, obtained from the ¹D_{NH} RDCs meas-

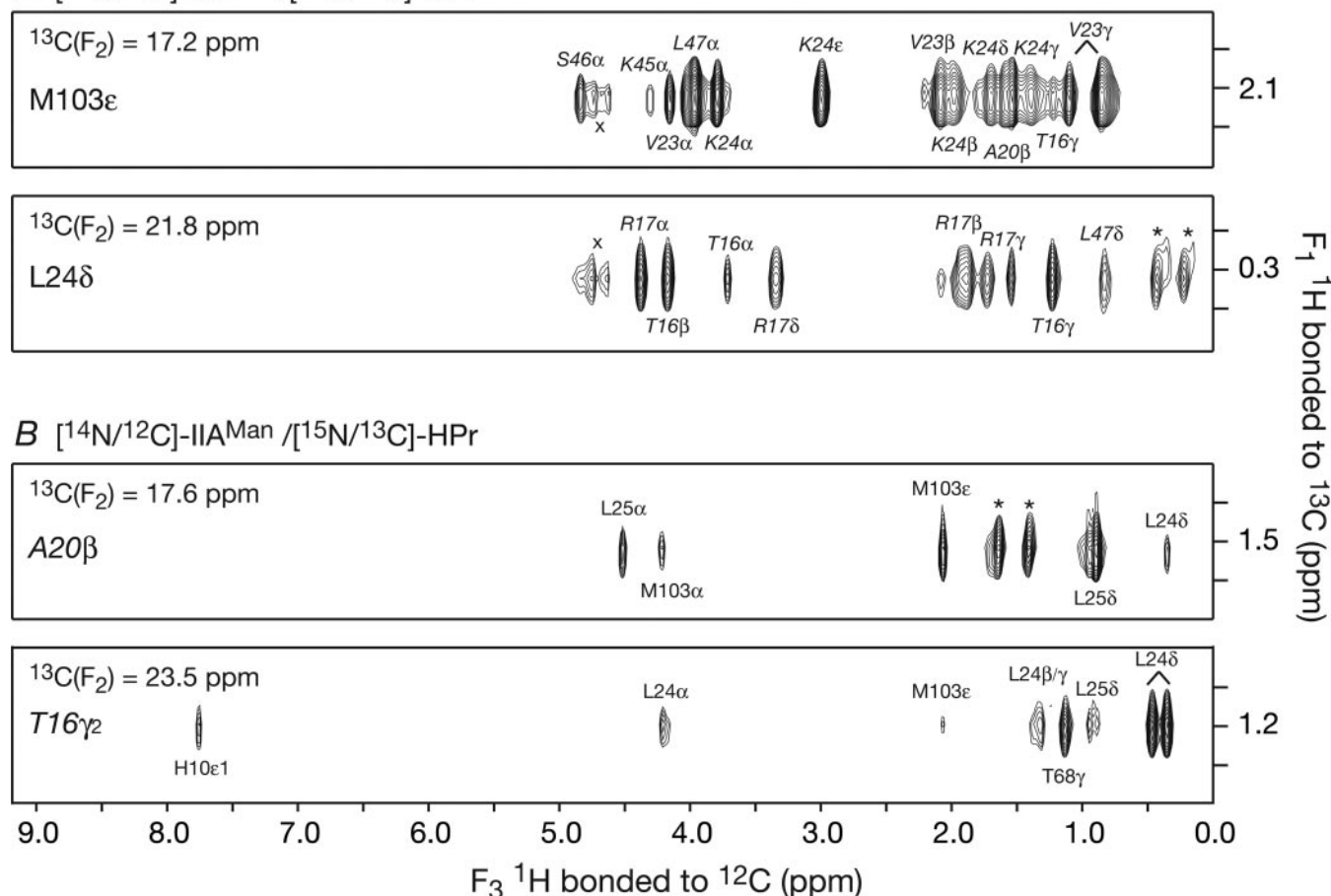
A [¹⁵N/¹³C]-IIA^{Man} / [¹⁴N/¹²C]-HPr

FIG. 2. **Intermolecular NOE in the IIA^{Man}-HPr complex.** Strips from three-dimensional ¹³C-separated/¹²C-filtered NOE spectra recorded on the IIA^{Man}-HPr complex with ¹⁵N/¹³C-labeled IIA^{Man} (A) and ¹⁵N/¹³C-labeled HPr (B) are shown, illustrating specifically intermolecular NOEs from protons attached to ¹³C on one protein to protons attached to ¹²C on the other. The asterisks denote residual diagonal (autocorrelation) peaks, and the peaks at ~4.7 ppm, indicated by × in A, arise from residual HOD. Residues of HPr are labeled in italics.

ured on labeled IIA^{Man} fully saturated with HPr using SVD against the 1.7 Å resolution crystal structure of IIA^{Man} (14). Thus, one can conclude that the back-calculated RDCs for HPr in the 1:2 IIA^{Man}(dimer)-HPr complex and the observed RDCs for labeled IIA^{Man} in the 1:2 IIA^{Man}(dimer)-HPr complex are described by a single alignment tensor.

Back-calculated ¹D_{NH} RDCs for HPr in a pure 1:2 IIA^{Man}-(dimer)-HPr complex can also be derived using calculated RDC values for free HPr, obtained by SVD against the x-ray structure coordinates of free HPr (17), instead of the observed values. The values of D_a^{NH} and η obtained in this manner are -28.3 Hz and 0.02, respectively, with $R_{dip}^{NH} = 11.3\%$ and $r_{corr} = 0.99$. The r.m.s. difference and correlation coefficient between the back-calculated RDCs for bound HPr derived using the two alternative approaches are 4.5 Hz (corresponding to an *R*-factor error of 8.9% (44)) and 0.99, respectively, and the slope of the linear fit is 0.98. Thus, both back-calculation methods are in excellent agreement with each other.

The rigid body/torsion angle-simulated annealing calculations were carried out using both sets of back-calculated ¹D_{NH} RDCs for bound HPr, with a single alignment tensor describing the IIA^{Man} and HPr components of the complex and compromise D_a^{NH} and η values of -28.2 Hz and 0.1, respectively. The two restrained regularized mean structures, each derived from an ensemble of 100 simulated annealing structures, deviate by only 0.08 Å for all backbone atoms, and the orientations of the two HPr molecules relative to the IIA^{Man} dimer differ by only 0.2°, which is well within the errors of the coordinates. Note

that the RDCs serve to orient not only HPr relative to IIA^{Man} but also the two bound HPr molecules in the complex relative to each other. A summary of the structural statistics is provided in Table I. A superposition of the backbone for the final ensemble of 100 simulated annealing structures is shown in Fig. 3A, and a reweighted atomic probability density map (40) for selected interfacial side chains is displayed in Fig. 3B.

Overall Description of the Complex—Two views of a ribbon diagram representation of the 48-kDa IIA^{Man}-HPr complex are shown in Fig. 4, A and B. IIA^{Man} is a symmetric, chain-swapped dimer with two symmetrically placed HPr binding sites on either side of the dimer. Each binding site is located at the interface of the two subunits, which form a relatively deep groove (~18 Å in length, 10 Å in width, and 6 Å in depth) on the surface of the IIA^{Man} dimer (Fig. 4, C and D). The total accessible surface area buried at each binding site is 1450 Å², of which 710 Å² originates from IIA^{Man} and 740 Å² from HPr. The interaction between IIA^{Man} and HPr predominantly involves helix-helix contacts (Fig. 4, E and F), specifically between helices $\alpha 1$ (residues 16–28) and $\alpha 2$ (residues 47–52) of HPr (henceforth, the use of italics for residue numbering refers specifically to HPr) and helices $\alpha 1$ (residues 13–25), $\alpha 4$ (residues 95–107), and $\alpha 5$ (residues 111–125) of one subunit of IIA^{Man} (denoted as subunit B and colored red in the figures). Helix $\alpha 1$ of HPr and helix $\alpha 4$ of IIA^{Man} interact along virtually their entire lengths and are oriented approximately parallel to each other (inter-helix angle at about -28°). In addition, helix $\alpha 1$ of HPr and helix $\alpha 1$ of IIA^{Man} are oriented approximately orthogonal to

TABLE I
Structural statistics

The notation of the NMR structures are as follows: (SA) are the final 100 simulated annealing structures, $\overline{\text{(SA)}}$, is the restrained regularized mean structure.

	(SA)	$\overline{\text{(SA)}}$
Number of experimental NMR restraints ^a		
Intermolecular interproton distance restraints	58 × 2	
IIA ^{Man} intrasubunit interproton distance restraints ^b	47 × 2	
IIA ^{Man} intersubunit interproton distance restraints ^b	16 × 2	
HPr intramolecular interproton distance restraints ^b	39 × 2	
IIA ^{Man} interfacial sidechain torsion angle restraints	16 × 2	
HPr interfacial sidechain torsion angle restraints	13 × 2	
IIA ^{Man} ¹ D _{NH} dipolar couplings	92 × 2	
HPr ¹ D _{NH} dipolar couplings	66 × 2	
r.m.s. deviation from interproton distance restraints (Å) ^c	0.005 ± 0.002	0.009
r.m.s. deviation from side-chain torsion angle restraints (°) ^c	0.15 ± 0.10	0
Overall dipolar couplings <i>R</i> -factor (%) ^d		
IIA ^{Man}	11.6 ± 0/11.6 ± 0	11.6/11.6
HPr	18.5 ± 0/12.4 ± 0	18.5/12.4
Measures of structural quality ^e		
Intermolecular repulsion energy (kcal · mol ⁻¹)	0.8 ± 0.5	0.6
Intermolecular Lennard-Jones energy (kcal · mol ⁻¹)	-22.3 ± 5.6	-16.7
Coordinate precision of the dimeric complex (Å) ^f		
Complete backbone (N, C α , C', O) atoms	0.13 ± 0.04	
Interfacial side chain heavy atoms	0.87 ± 0.07	

^a The factor 2 relates to the fact that the restraints are duplicated because the structure is a symmetric dimer. In the context of the dipolar couplings, this enforces symmetry of the two halves of the complex and serves to orient the two molecules of HPr relative to each other, in addition to orienting the HPr molecules relative to the IIA^{Man} dimer.

^b The intramolecular NOE-derived interproton distance restraints relate only to interfacial side chains.

^c None of the structures exhibit interproton distance violations >0.3 Å or torsion angle violations >5°.

^d The dipolar couplings are refined using a single alignment tensor for the whole complex. The dipolar coupling *R*-factor, which scales between 0 and 100%, is defined as the ratio of the r.m.s. deviation between observed and calculated values to the expected r.m.s. deviation if all the N-H vectors were randomly distributed (42). The latter is given by $(2D_a^2 [4+3\eta^2]/5)^{1/2}$ where D_a is the magnitude of the axial component of the alignment tensor and η the rhombicity. The values of D_a^{NH} and η used in the calculations (see the "Results") are -28.2 Hz and 0.1, respectively. Two values for the dipolar coupling *R*-factors are listed corresponding to two separate sets of simulated annealing calculations (100 structures each) with the ¹D_{NH} RDCs for HPr in the pure 1:2 IIA^{Man} (dimer)-HPr complex back-calculated from the experimental RDCs measured on a sample comprising a 3-fold excess of labeled HPr over IIA^{Man} subunits in combination with either the experimental or calculated RDCs for free HPr (with the latter derived from SVD best-fitting the experimental RDCs for free HPr to the free HPr crystal structure; see text). The same set of experimental RDCs for IIA^{Man} in the complex is employed for both sets of structure calculations. For reference, using the values of D_a^{NH} and η given above, an SVD best-fit of the RDCs against the individual x-ray structures yields the same dipolar coupling *R*-factors as listed in the table for the complex.

^e The intermolecular repulsion energy is given by the value of the quartic van der Waals repulsion term calculated with a force constant of 4 kcal · mol⁻¹ · Å⁻⁴ and a van der Waals radius scale factor of 0.78. The intermolecular Lennard-Jones van der Waals interaction energy is calculated using the CHARMM19/20 parameters and is not included in the target function used to calculate the structures. The percentage of residues present in the most favorable region of the Ramachandran map (50) is 96.4% for the x-ray structure of IIA^{Man} (Protein Data Bank Code 1PDO) and 93.3% for the x-ray structure of HPr (1POH) and 96.4%.

^f Defined as the average r.m.s. difference between the final 100 simulated annealing structures and the mean coordinates. The value quoted for the complete backbone provides only a measure of the precision with which the orientation and translation of the two HPr molecules relative to the IIA^{Man} dimer have been determined and does not take into account the accuracy of the x-ray coordinates of IIA^{Man} and HPr. The latter is likely to be around 0.3 Å judging from the crystallographic resolution and *R*-factors.

each other (interhelical angle at about -70°) with contacts between the N-terminal end of the former and the C-terminal end of the latter. Helix α_2 of HPr is oriented antiparallel to helix α_4 (interhelical angle ~136°) and parallel to helix α_5 (interhelical angle ~21°) of IIA^{Man}. Contacts occur along the full-length of helix α_2 of HPr, but because it is so short, contacts are limited to the N-terminal end of helix α_4 and the C-terminal end of helix α_5 of IIA^{Man}. The second subunit of IIA^{Man} (denoted as subunit A and colored *blue* in the figures) contributes the active site His-10, located in the turn (residues 9–12) between strand β_1 and helix α_1 ; the loop (residues 35–41) connecting strand β_2 and helix α_2 ; and the N-terminal end of helix α_3 (residues 72–81). The latter is involved in an end-to-end interaction with the N- and C-terminal ends of helices α_1 and α_2 , respectively, of HPr.

The IIA^{Man}-HPr Interface—A stereoview of the interface is shown in Fig. 5A, a summary of the intermolecular contacts in Fig. 5B, and surface representations in Fig. 5, C and D. The interaction surface on IIA^{Man} is ellipsoid in shape, ~33 Å long and 23 Å wide, whereas that on HPr is closer to circular (25 Å in length and 23 Å in width). The two surfaces are complementary, concave for IIA^{Man} and convex for HPr. The interface comprises 27 residues from IIA^{Man}, 12 from subunit A (denoted

as the subunit contributing the active site His-10) and 15 from subunit B, and 17 residues from HPr (Fig. 5B). The interface is predominantly hydrophobic in nature, with 59% of the atoms being non-polar and 41% polar. The hydrophobic residues are located at the center of the interface surrounded by a partial ring of polar uncharged residues on top and a partial outer ring of charged residues at the bottom, negatively charged in the case of IIA^{Man} (Fig. 5C) and positively charged for HPr (Fig. 5D). It is interesting to note that, excluding the charged residues located exclusively at the periphery of the binding site, the bottom half of the interaction surface is predominantly hydrophobic, whereas the top half is predominantly polar. In the case of the binding site on IIA^{Man}, the majority of hydrophobic residues originate from subunit B, whereas the polar ones, including the active site His-10, are predominantly from subunit A. There are extensive interactions between Met-23^B, Leu-24^B, Leu-25^B, Pro-96^B, and Gly-125^B of subunit B of IIA^{Man} and Ala-20, Val-23, Leu-47, and Phe-48 of HPr.

There are a number of potential electrostatic and hydrogen-bonding (direct or water mediated) interactions that presumably contribute to the specificity of the interaction and serve to orient HPr relative to IIA^{Man}. The three negatively charged residues at the bottom end of the binding surface of IIA^{Man}

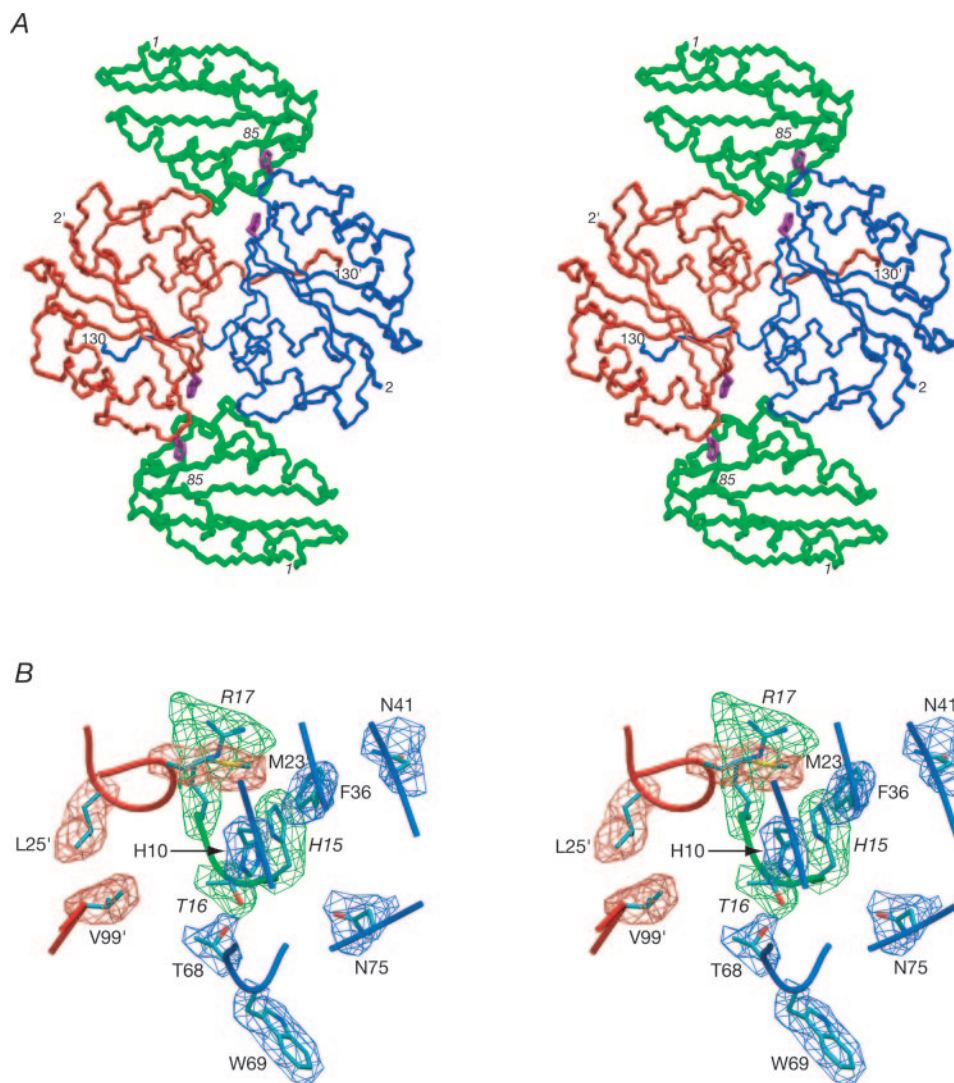


FIG. 3. **Solution structure of the IIA^{Man}-HPr complex.** A, best-fit superimposition of the backbone (N, C α , and C atoms) of the 100 final simulated annealing structures with HPr in green and subunits A and B of IIA^{Man} in blue and red, respectively. The side chains of the active site histidines, His-10 of IIA^{Man} and His-15 of HPr, from the restrained regularized mean structure are shown in purple. B, isosurface of the reweighted atomic density probability map (40) for selected side chains drawn at a value of 25% maximum calculated from the 100 simulated annealing structures. The color scheme used in A is also used for the atomic probability density map grid. The backbone of the restrained regularized mean structure is shown as a tube with the same color scheme as in A, and the side-chain coordinates within the atomic density map are colored on the basis of atom type (cyan, carbon; blue, nitrogen; and red, oxygen). Residues of HPr are labeled in *italics*.

(Fig. 5C) participate in electrostatic interactions. There is a pair of salt bridges between the side chains of Asp-106^B of IIA^{Man} and Lys-24 of HPr and between Asp-107^B and Lys-27, and there is an electrostatic interaction between the carboxylate group of Glu-100^B and the hydroxyl group of Ser-46. At the center of the interface, there is a hydrogen bond between the hydroxyl groups of Thr-68^A of IIA^{Man} and Thr-16 of HPr and electrostatic interactions between the side chain of Lys-127^B of IIA^{Man} and the side chains of Gln-51 and Thr-52 of HPr. Finally, at the top edge of the binding surface, there is a potential electrostatic interaction network involving Arg-79^A and Asn-75^A of IIA^{Man} and Asn-12 of HPr. In addition, there are a few potential side chain-backbone electrostatic interactions; these, specifically, are between the side chain of Arg-17 HPr and the backbone carbonyl of Met-23^B of IIA^{Man}, the side chain of Gln-21 and the backbone carbonyl of Leu-24^B, and the N- ϵ 1H of the Trp-69^A side chain and the backbone carbonyl of Gln-51. A comparison with the sequences of *E. coli* IIA^{fructose} (45) and *Klebsiella pneumoniae* IIA^{sorbitose} (46), which belong to the IIA^{Man} family of enzymes II permeases, reveals conservation of Asn-75, Glu-100, and Asp-106, suggesting that the electrostatic

interactions described above involving these three residues may play an important role in specificity.

Comparison of Other HPr Complexes with PTS Proteins—We have previously solved the structures of the enzyme I N-terminal domain (EIN)-HPr (5), IIA^{Glc}-HPr (6), and IIA^{Mtl}-HPr (8) complexes. The buried accessible surface area at the protein-protein interface for the complexes with members of the three different families of enzymes II are comparable, ranging from 1365 Å² for the IIA^{Glc}-HPr complex (6) to 1450 Å² for both the IIA^{Mtl}-HPr (8) and IIA^{Man}-HPr complexes (current work). The buried accessible surface area of these complexes is ~25–30% smaller than that at the interface of the EIN-HPr complex (5). The interaction surfaces are similar on HPr in all four complexes although somewhat more extensive in the case of the EIN-HPr complex. However, the structural elements comprising the interaction surfaces on the partner PTS proteins are very different. In the cases of EIN (5) and IIA^{Man}, the binding surface is either entirely or predominantly helical, respectively. For IIA^{Glc}, it is mainly β -sheet (6), and for IIA^{Mtl}, there is a mix of sheet and helices (8). Although the binding surface on IIA^{Man} is composed largely of helices (Figs. 4 and 5), it differs in two

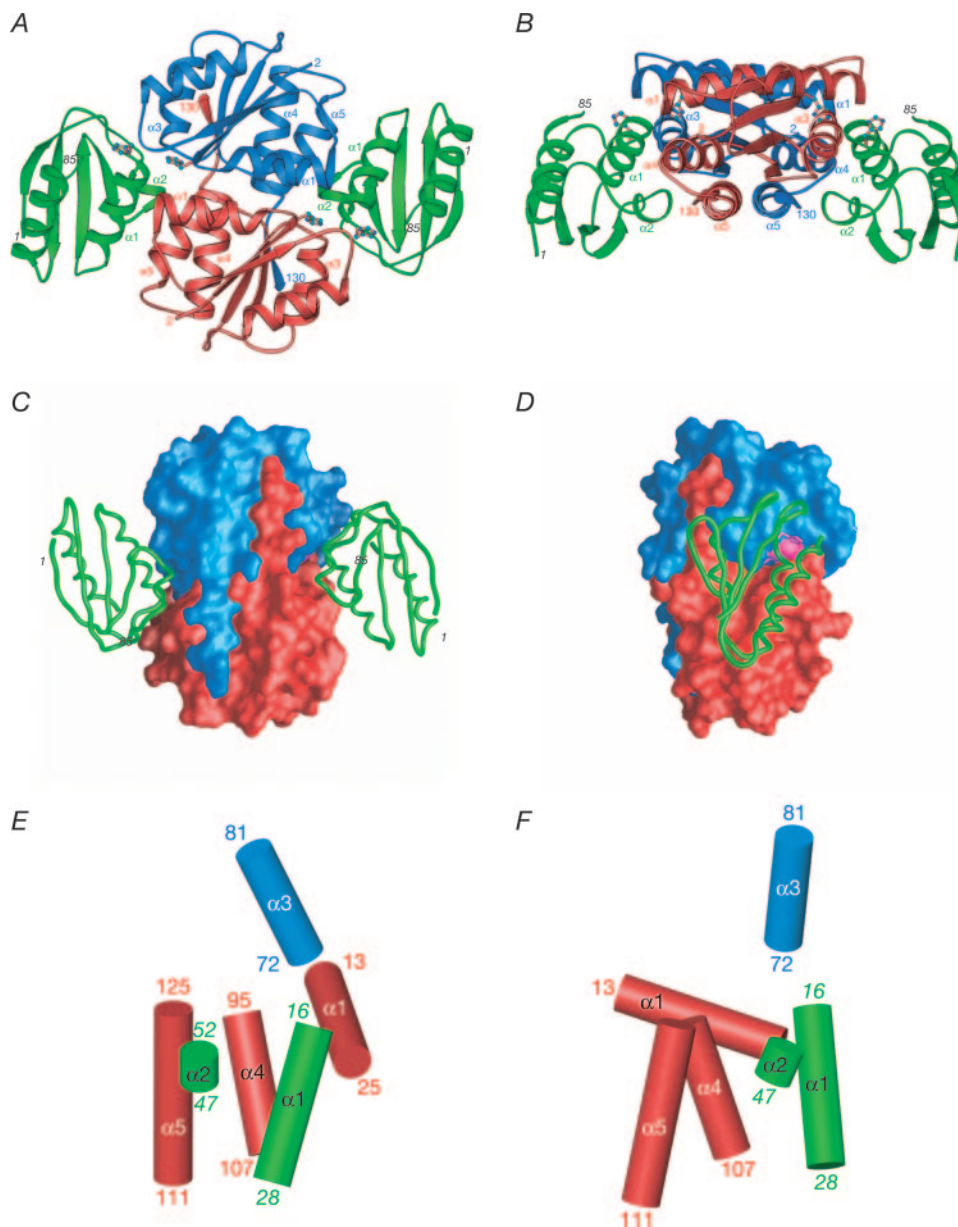


FIG. 4. **Overall interaction of HPr and IIA^{Man}.** A and B, ribbon diagrams of two orthogonal views of the IIA^{Man}-HPr complex with the side chains of the active site histidines (*His-10* of IIA^{Man} and *His-15* of HPr) depicted as bonds, with carbon atoms in cyan and nitrogen atoms in blue. C and D, two orthogonal views of a surface representation of IIA^{Man} illustrating the groove formed at the interface of the two subunits in which HPr (depicted as a tube) binds. The view in C is rotated 180° relative to that in A. E and F, two orthogonal views illustrating helix-helix packing at the IIA^{Man}-HPr interface, with the helices represented by idealized cylinders. HPr is shown in green, and subunits A and B of IIA^{Man} in blue and red, respectively. In E and F, the active site *His-10* of IIA^{Man} that interacts with the displayed HPr molecule is located in subunit A (blue). Residues of HPr are labeled in italics.

significant aspects with regard to that of EIN. First, the binding surface on IIA^{Man} originates from two separate subunits, whereas that on EIN is derived from the helical domain of a two-domain single-chain protein. (Note, however, that the active site histidine on EIN is located on the α/β domain and represents the only site of close proximity on that domain to HPr.) Second, the disposition of the interacting helices of EIN is quite different from that in IIA^{Man}. A comparison of the orientation of the interacting helices of EIN and IIA^{Man} relative to helices $\alpha 1$ and $\alpha 2$ of HPr is shown in Fig. 6, where it is clear that the helices of IIA^{Man} are approximately orthogonal to those of EIN. Despite the considerable differences in the underlying structural elements, the shape and composition of the interaction surfaces for HPr on IIA^{Man}, EIN, IIA^{Glc}, and IIA^{Mtl} are broadly similar. In addition, it is interesting to note that the cluster of negative residues at the bottom of the interaction

surface on IIA^{Man} (Fig. 5) is preserved in the other three complexes (*cf.* Figs. 6 in Refs. 6 and 8). Thus, the Glu-100, Asp-106, and Asp-107 triad on IIA^{Man} has its approximate equivalent in Asp-82, Glu-83, and Glu-84 for EIN; Glu-80, Glu-86, and Asp-144 for IIA^{Glc}; and Glu-59 and Asp-123 for IIA^{Mtl}.

Modeling the Phosphoryl Transition State Intermediate—Phosphoryl transfer occurs from the N- $\delta 1$ atom of *His-15* of HPr to the N- $\epsilon 2$ atom of *His-10* of IIA^{Man} (11). As in all other PTS complexes, the transition state involves a pentacoordinate phosphoryl group in a trigonal bipyramidal geometry (47, 48). To model the phosphoryl transition state, we used a strategy similar to one described previously (5–8), in which conjoined rigid body/cartesian coordinate restrained minimization is applied to the restrained regularized mean coordinates of the complex subject to geometric restraints related to the phosphoryl group in conjunction with all of the experimental NMR

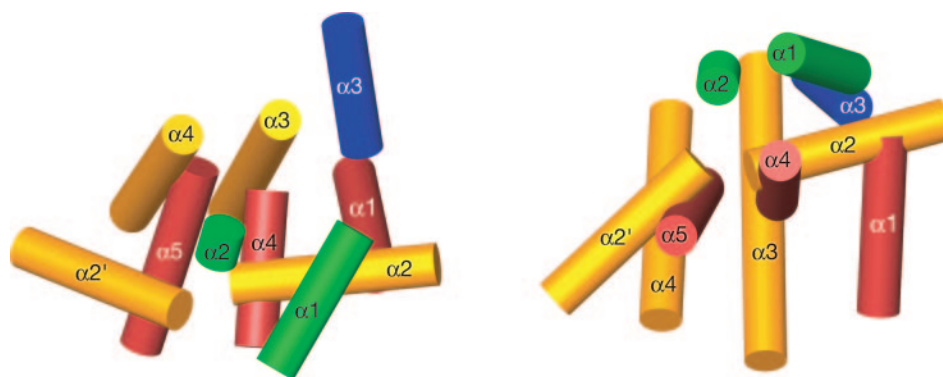


FIG. 6. Comparison of the relative orientation of the interacting helices in the IIA^{Man}-HPr and EIN-HPr complexes. The two complexes have been best-fitted to the coordinates of HPr. Two approximately orthogonal views are shown with the helices of HPr ($\alpha 1$ and $\alpha 2$) in green; helices $\alpha 1$, $\alpha 4$, and $\alpha 5$ of subunit B of IIA^{Man} in red; helix $\alpha 3$ of subunit A of IIA^{Man} in blue; and helices $\alpha 2$, $\alpha 2'$, $\alpha 3$, and $\alpha 4$ of EIN in gold. The coordinates of the EIN-HPr complex are taken from Ref. 5 (Protein Data Bank accession code 3EZA).

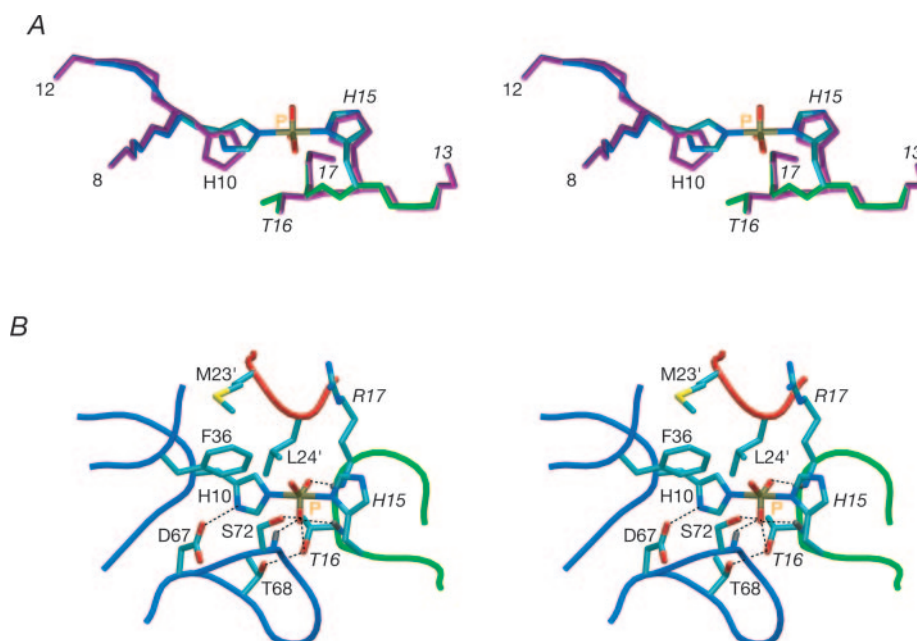


FIG. 7. The phosphoryl transition state of the IIA^{Man}-HPr complex. **A**, stereoview of the active site histidines and the backbone in their immediate vicinity in the unphosphorylated state and the putative associative transition state complex. The backbone (N, C α , and C atoms of residues 8–12 of subunit A of IIA^{Man} and residues 13–17 of HPr), the side chains of the active site histidines, and the side chain of Thr-16 of HPr in the unphosphorylated state are shown in purple. The backbone and the side chain of Thr-16 are shown in green for the associative transition state complex. In the transition state complex, the active site histidines and the pentacoordinate phosphoryl group in a trigonal bipyramidal geometry are color-coded on the basis of atom type (cyan, carbon; blue, nitrogen; red, oxygen; and gold, phosphorus). The N- $\epsilon 2$ (His-10)-P and N- $\delta 1$ (His-15)-P distances in the associative transition state complex are 2 Å, which is completely consistent with the trigonal bipyramidal geometry of the phosphoryl group. Note that the transition state can be formed with minimal perturbation to the backbone. **B**, detailed view of the transition state complex. The backbone is shown as a tube with HPr in green and subunits A and B of IIA^{Man} in blue and red, respectively. The side chains are color-coded on the basis of atom type (cyan, carbon; blue, nitrogen; red, oxygen; gold, phosphorus; and gray, hydrogen, for the backbone amide of Thr-16). Potential hydrogen-bonding interactions are depicted as dashed lines. Residues of HPr are labeled in italics.

restraints. The only portion of the complex allowed to move upon minimization comprises the backbone and side chains of the active site histidines and the adjacent residues on either side (*i.e.* residues 9–11 of IIA^{Man} and 14–16 of HPr) and the interfacial side chains. An associative transition state complex (Fig. 7A) with nitrogen-phosphorus distances of 2 Å is readily accommodated with minimal atomic r.m.s. shifts (<0.3 Å for

the backbone of residues 9–11 of IIA^{Man} and 14–16 of HPr). The $g^-(\chi_1)/g^+(\chi_2)$ and $g^+(\chi_1)/g^+(\chi_2)$ side-chain conformations of His-10 and His-15, respectively, are maintained in the transition state, and the phosphorus atom lies in the plane of both imidazole rings. A dissociative transition state with nitrogen-phosphorus distances of 3 Å, however, can only be accommodated with the phosphorus atom out of the plane of the imid-

involved in potential electrostatic, hydrogen-bonding, or water-mediated hydrogen-bonding interactions are indicated in red (side chain-side chain contacts), blue (side chain of HPr to backbone carbonyl of IIA^{Man}), or green (side chain of IIA^{Man} to backbone carbonyl of HPr). The active site histidines are shown in purple. **C**, interaction surface on IIA^{Man} for binding HPr. **D**, interaction surface on HPr for binding IIA^{Man}. Residues in the interaction surfaces (**C** and **D**) are color-coded as hydrophobic (green), hydrophilic (cyan), positively charged (blue), or negatively charged (red). The relevant portions of the backbone of the interacting partner, HPr in **C** (gold) and IIA^{Man} in **D** (lilac for subunit A, gold for subunit B), are displayed as tubes. In **C**, the surface of the non-interacting residues of IIA^{Man} is colored in dark gray for subunit A and light gray for subunit B. Residues of HPr are labeled in italics.

azole ring of His-10. This suggests that in the case of the IIA^{Man}-HPr complex, an associative transition state mechanism is more likely.

The phosphoryl group and active site histidines lie on a bed of hydrophobic residues comprising Met-23^B and Leu-24^B of subunit B of IIA^{Man}, Phe-36^A and the methyl group of Thr-68^A of subunit A of IIA^{Man}, and the methyl group of Thr-16 and the hydrophobic portion of the side chain of Arg-17 of HPr. In the case of the IIA^{Glc}-HPr complex, the guanidino group of Arg-17, a highly conserved residue on HPr, neutralizes two spatially proximal carboxylates (Asp-38 and Asp-94) on IIA^{Glc} and has been shown to be critical for phosphoryl transfer. In both the IIA^{Man}-HPr and IIA^{Mtl}-HPr complexes, however, the guanidino group of Arg-17 is exposed to solvent, and it is largely the hydrophobic portion of the side chain that participates in intermolecular interactions.

The nucleophilicity of His-10 is increased by an intramolecular hydrogen-bonding interaction between the N- δ 1 atom of His-10^A and the carboxylate of Asp-67^A (Fig. 7B). The phosphoryl group is hydrogen-bonded to the hydroxyl group of Thr-16 and the backbone amides of Thr-16 and Arg-17 on the HPr side and to the hydroxyl group of Ser-72^A and the backbone amide of Ser-72^A on the IIA^{Man} side (Fig. 7B). In addition, the positive helix macrodipoles (49) at the N terminus of helix α 3 of IIA^{Man} and helix α 1 of HPr serve to partially neutralize the negatively charged phosphoryl group. The importance of the hydroxyl group of Ser-72 is supported by mutation of Ser-72 to Cys, which reduces the activity of IIA^{Man} to only 6% of wild type (13), and by the observation that the hydroxyl group is preserved in the form of Ser or Thr in the related enzymes IIA^{sorbitose} and IIA^{fructose}.

Concluding Remarks—In this study, we have solved the solution NMR structure of the 48-kDa IIA^{Man}-HPr dimeric complex. RDCs were critical to accurately orient both HPr to IIA^{Man} and the two bound HPr molecules to each other. Because binding is relatively weak, the dipolar couplings for HPr in a 1:2 IIA^{Man}(dimer)-HPr complex had to be back-calculated from the RDCs measured on free HPr and a sample containing an excess of HPr over IIA^{Man}. This procedure, however, still results in accurate RDCs for the bound state of HPr. This accuracy is evidenced by both the low dipolar coupling *R*-factor for the back-calculated RDCs when they were best-fitted to the coordinates of the crystal structure of free HPr and by the coincidence of the magnitude and rhombicity of the back-calculated alignment tensor with those of IIA^{Man}, derived directly from the RDCs measured on IIA^{Man} fully saturated with HPr.

Although the structure of the unphosphorylated IIA^{Man}-HPr complex was solved (phosphorylated histidine in the context of a phosphoryl transfer complex is too labile to permit structural studies), an associative phosphoryl transition state complex could readily be modeled on the basis of the structure with minimal shifts in atomic coordinates, limited to the active site histidines and the immediately adjacent residues on either side. Thus, phosphoryl transfer can proceed with maximum energetic efficiency without any significant conformational changes in either partner protein.

The interaction surface on HPr for IIA^{Man} is similar to and overlaps considerably with that used by HPr to recognize three other members of the PTS, enzymes I, IIA^{Glc}, and IIA^{Mtl}, for which complexes with HPr have been solved previously (5, 6, 8). Despite the fact that the underlying structural elements composing the interaction surface for HPr on IIA^{Man} are entirely different from those on EIN, IIA^{Glc}, and IIA^{Mtl} (either in terms of secondary structure or the arrangement of the various secondary structural elements), the interaction surfaces for HPr on all four proteins have a number of features in common. These include general shape, residue composition, and overall

spatial disposition of hydrophobic, hydrophilic, and charged residues. The interaction surfaces, however, are not identical and allow for considerable redundancy of interactions, which is a critical element in permitting HPr to specifically recognize so many structurally diverse proteins.

Acknowledgments—We thank Drs. Dan Garrett and Frank Delaglio for software and technical support.

REFERENCES

- Kundig, W., Ghosh, S., and Roseman, S. (1964) *Proc. Natl. Acad. Sci. U. S. A.* **52**, 1067–1074
- Postma, P. W., Lengeler, J. W., and Jacobson, G. R. (1993) *Microbiol. Rev.* **57**, 543–594
- Robillard, G. T., and Broos, J. (1999) *Biochim. Biophys. Acta* **1422**, 73–104
- Siebold, C., Flükiger, K., Beutler, R., and Erni, B. (2001) *FEBS Lett.* **504**, 104–111
- Garrett, D. S., Seok, Y.-J., Peterkofsky, A., Gronenborn, A. M., and Clore, G. M. (1999) *Nat. Struct. Biol.* **6**, 166–173
- Wang, G., Louis, J. M., Sondej, M., Seok, Y.-J., Peterkofsky, A., and Clore, G. M. (2000) *EMBO J.* **19**, 5635–5649
- Cai, M., Williams, D. C., Wang, G., Lee, B. R., Peterkofsky, A., and Clore, G. M. (2003) *J. Biol. Chem.* **278**, 25191–25206
- Cornilescu, G., Lee, B. R., Cornilescu, C., Wang, G., Peterkofsky, A., and Clore, G. M. (2002) *J. Biol. Chem.* **277**, 42289–42298
- Erni, B., and Zanolari, B. (1985) *J. Biol. Chem.* **260**, 15495–15503
- Erni, B., Zanolari, B., and Kocher, H. P. (1987) *J. Biol. Chem.* **262**, 5238–5247
- Erni, B., Zanolari, B., Graff, P., and Kocher, H. P. (1989) *J. Biol. Chem.* **264**, 18733–18741
- Markovic-Housley, Z., Cooper, A., Lustig, A., Flükiger, K., Stolz, B., and Erni, B. (1994) *Biochemistry* **33**, 10977–11094
- Stolz, B., Huber, M., Markovic-Housley, Z., and Erni, B. (1993) *J. Biol. Chem.* **268**, 27094–27099
- Nunn, R. S., Markovic-Housley, Z., Genovesio-Taverne, J.-C., Flükiger, K., Rizkallah, P. J., Jansonius, J. N., Schimer, T., and Erni, B. (1996) *J. Mol. Biol.* **259**, 502–511
- Schauder, S., Nunn, R. S., Lanz, R., Erni, B., and Schirmer, T. (1998) *J. Mol. Biol.* **276**, 591–602
- Orriss, G. L., Erni, B., and Schirmer, T. (2003) *J. Mol. Biol.* **327**, 1111–1119
- Jia, Z., Quail, J. W., Waygood, E. B., and Delbaere, L. T. (1993) *J. Biol. Chem.* **268**, 22490–22501
- Clore, G. M. (2000) *Proc. Natl. Acad. Sci. U. S. A.* **97**, 9021–9025
- Schwieters, C. D., and Clore, G. M. (2001) *J. Magn. Reson.* **152**, 288–302
- Garrett, D. S., Seok, Y.-J., Peterkofsky, A., Clore, G. M., and Gronenborn, A. M. (1997) *Biochemistry* **36**, 4393–4398
- Goto, N. K., Gardner, K. H., Mueller, G. A., Willis, R. C., and Kay, L. E. (1999) *J. Biomol. NMR* **13**, 369–374
- Delaglio, F., Grzesiek, S., Vuister, G. W., Zhu, G., Pfeifer, J., and Bax, A. (1995) *J. Biomol. NMR* **6**, 277–293
- Garrett, D. S., Powers, R., Gronenborn, A. M., and Clore, G. M. (1991) *J. Magn. Reson.* **95**, 214–220
- Clore, G. M., and Gronenborn, A. M. (1991) *Science* **252**, 1390–1399
- Bax, A., and Grzesiek, S. (1993) *Acc. Chem. Res.* **26**, 131–138
- Clore, G. M., and Gronenborn, A. M. (1998) *Trends Biotechnol.* **16**, 22–34
- Bax, A., Vuister, G. W., Grzesiek, S., Delaglio, F., Wang, A. C., Tschudin, R., and Zhu, G. (1994) *Methods Enzymol.* **239**, 79–105
- Pelton, J. G., Torchia, D. A., Meadow, N. D., and Roseman, S. (1993) *Protein Sci.* **2**, 543–558
- Ruckert, M., and Otting, G. (2000) *J. Am. Chem. Soc.* **122**, 7793–7797
- Peruvshin, K., Riek, R., Wider, G., and Wüthrich, K. (1997) *Proc. Natl. Acad. Sci. U. S. A.* **94**, 12366–12371
- Tugarinov, V., Muhandiram, R., Ayed, A., and Kay, L. E. (2002) *J. Am. Chem. Soc.* **124**, 10025–10035
- Schwieters, C. D., Kuszewski, J., Tjandra, N., and Clore, G. M. (2003) *J. Magn. Reson.* **160**, 65–73
- Clore, G. M., and Gronenborn, A. M. (1998) *Proc. Natl. Acad. Sci. U. S. A.* **95**, 5891–5898
- Clore, G. M., and Kuszewski, J. (2002) *J. Am. Chem. Soc.* **124**, 2866–2867
- Kuszewski, J., Gronenborn, A. M., and Clore, G. M. (1999) *J. Am. Chem. Soc.* **121**, 2337–2338
- Zweckstetter, M., and Bax, A. (2000) *J. Am. Chem. Soc.* **122**, 3791–3792
- Schwieters, C. D., and Clore, G. M. (2001) *J. Magn. Reson.* **149**, 239–244
- Carson, M. (1991) *J. Appl. Crystallogr.* **24**, 958–961
- Nicholls, A., Sharp, K. A., and Honig, B. (1991) *Proteins* **11**, 281–296
- Schwieters, C. D., and Clore, G. M. (2002) *J. Biomol. NMR* **23**, 221–225
- Bax, A., Kontaxis, G., and Tjandra, N. (2001) *Methods Enzymol.* **339**, 127–174
- Clore, G. M., and Garrett, D. S. (1999) *J. Am. Chem. Soc.* **121**, 9008–9012
- Williams, D. C., Cai, M., and Clore, G. M. (2004) *J. Biol. Chem.* **279**, 1449–1457
- Clore, G. M., and Schwieters, C. D. (2004) *J. Am. Chem. Soc.* **126**, 2923–2938
- Martin-Verstrate, I., Debarbouille, M., Klier, A., and Rapoport, G. (1990) *J. Mol. Biol.* **214**, 657–671
- Wehmeier, U. F., and Lengeler, J. W. (1994) *Biochim. Biophys. Acta* **1208**, 348–351
- Begley, G. S., Hansen, D. E., Jacobson, G. R., and Knowles, J. R. (1982) *Biochemistry* **21**, 5552–5556
- Mueller, E. G., Khandekar, S. S., Knowles, J. R., and Jacobson, G. R. (1990) *Biochemistry* **29**, 6892–6896
- Hol, W. G. J., van Duijn, P. T., and Berendsen, H. J. C. (1978) *Nature* **273**, 443–446
- Laskowski, R. A., MacArthur, M. W., Moss, D. S., and Thornton, J. M. (1993) *J. Appl. Crystallogr.* **26**, 283–291